side of the common carotid artery and calculated their average (the average of the maximum common carotid IMT). We also measured the maximum IMT from the common carotid artery to the internal carotid artery on each side and averaged the results (the average of the maximum IMT). An atheromatous plaque was defined as a lesion with an IMT greater than or equal to 1.1 mm. We calculated plaque number by counting the numbers of plaques in both carotid arteries. To assess the severity of atherosclerosis, we used plaque score, which was calculated by summing all plaque thicknesses in both carotid systems.[18]

To examine the influence of patients' age on the percent plaque area, we divided them into 2 groups in the boundary of their median age (>62 and <62 years old). Hypertension was defined as systolic blood pressure greater than 140 mm Hg, diastolic blood pressure greater than 90 mm Hg, or current use of antihypertensive agents. Diabetes mellitus was defined as a hemoglobin A1C concentration greater than 6.5% or current use of hypoglycemic medications. Hypercholesterolemia was defined as total cholesterol concentration greater than 220 mg/dL or current use of cholesterol-lowering agents. Patients were categorized as smokers if they were current smokers.

The relationship between left main coronary artery atherosclerosis and carotid atherosclerosis was evaluated by simple linear regression analysis. Data were analyzed by StatView for Windows, version 5.0 (SAS Institute Inc, Cary, NC). The association between age, sex, presence of vascular risk factors, and percent plaque area in the left main coronary artery was examined by an unpaired t test. Multiple linear regression analyses were performed to determine atherosclerotic risk factors and carotid artery measurements that were significantly related to left main coronary artery atherosclerosis.

Results

The numbers of patients with hypertension, diabetes mellitus, and hypercholesterolemia and who were current smokers were 27 (60%), 21 (46.7%), 26 (57.8%), and 21 (46.7%), respectively. According to coronary angiography, 1-vessel disease was observed in 18 patients; 2-vessel disease was observed in 15 patients; and 3-vessel disease was observed in 12 patients. The mean percent plaque area ± SD was 34.1% ± 15.0%, and maximum percent plaque area was 37.5% ± 16.0%. The average of the maximum common carotid IMT, the average of the maximum IMT, plaque score, and plaque number were 0.98 ± 0.36 mm, 1.53 ± 0.88 mm, 4.26 ± 2.74 mm, and 2.4 ± 1.7, respectively. Significant differences in carotid ultrasonographic results were not observed among groups of patients with 1-, 2-, and 3-vessel disease.

There was no significant relationship between the mean percent plaque area, maximum percent plaque area, and patient's age (Table 1). The mean percent plaque area and maximum percent plaque area in men were increased significantly compared with those in women. The mean percent plaque area and maximum percent plaque area in patients with hypertension were also higher than those without hypertension. The mean percent plaque area and maximum percent plaque area did not differ statistically according to the presence of diabetes mellitus, hypercholesterolemia, or current smoking.

The average of the maximum common carotid IMT was correlated with both the mean percent plaque area and maximum percent plaque area on the basis of simple regression analysis (Table 2 and Figure 2). However, the average of the maximum IMT and plaque score did not significant-

Table 1. Mean and Maximum Percent Plaque Area by Patients' Clinical Characteristics

Characteristic	Mean %PA		Max %PA	
	Mean	*P*	Mean	*P*
Age				
<62 y	33.6		36.9	
>62 y	34.5	.85	37.9	.84
Sex				
Male	35.7		39.2	
Female	20.9	.036	23.5	.037
Hypertension				
Presence	38.3		40.9	
Absence	27.6	.017	32.3	.077
Diabetes mellitus				
Presence	31.0		34.4	
Absence	36.8	.20	40.2	.23
Hypercholesterolemia				
Presence	33.4		37.3	
Absence	34.9	.75	37.6	.95
Smoking habit				
Presence	34.6		39.0	
Absence	32.9	.73	32.9	.33

Max %PA indicates maximum percent plaque area; and Mean %PA, mean percent plaque area.

Table 2. Mean and Maximal Percent Plaque Area by Carotid Ultrasonographic Parameters

Parameter	Mean %PA		Max %PA	
	r	*P*	*r*	*P*
Max IMT-C avg, mm	0.39	.007	0.41	.005
Max-IMT avg, mm	0.14	.36	0.16	.30
PS, mm*	0.18	.22	0.22	.15
PN*	0.32	.034	0.35	.021

Max-IMT avg indicates average maximum IMT from the common carotid artery to the internal carotid artery on each side; Max IMT-C avg, average maximum IMT of each side of the common carotid artery; Max %PA, maximum percent plaque area; Mean %PA, mean percent plaque area; PN, plaque number; and PS, plaque score.
*Spearman rank correlation.

Figure 2. Scattergram of mean percent plaque area (mean %PA) and maximum percent plaque area (max %PA) by average maximum IMT of each side of the common carotid artery (max IMT-C avg). The max IMT-C avg was correlated with both mean %PA and max %PA on the basis of simple regression analysis (mean %PA: $r = 0.39$; $P = .007$; max %PA: $r = 0.41$; $P = .005$).

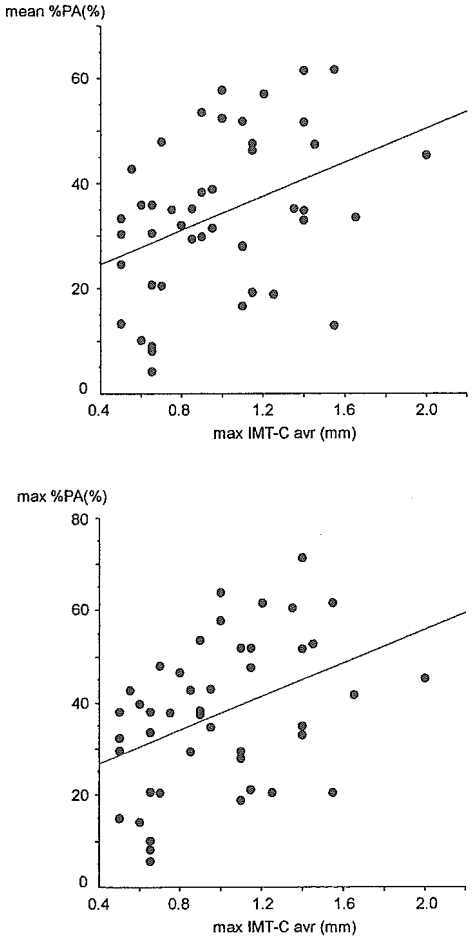

ly correlate with the mean percent plaque area or maximum percent plaque area. Plaque number was correlated with the mean percent plaque area and maximum percent plaque area (Figure 3). The average of the maximum common carotid IMT, average of the maximum IMT, plaque score, and plaque number of patients with calcifications in the left main coronary artery did not differ from those without calcifications.

All clinical and carotid ultrasonographic parameters with a significant relationship with the mean percent plaque area and maximum percent plaque area were tested with multivariate analysis (Table 3). Male sex, patients with hypertension, and the average of the maximum common carotid IMT were correlated with both the mean percent plaque area and maximum percent plaque area.

Figure 3. Scattergram of mean percent plaque area (mean %PA) and maximum percent plaque area (max %PA) by plaque number (PN). The PN was correlated with both mean %PA and max %PA on the basis of Spearman rank correlation (mean %PA: $r = 0.32$; $P = .034$; max %PA: $r = 0.35$; $P = .021$).

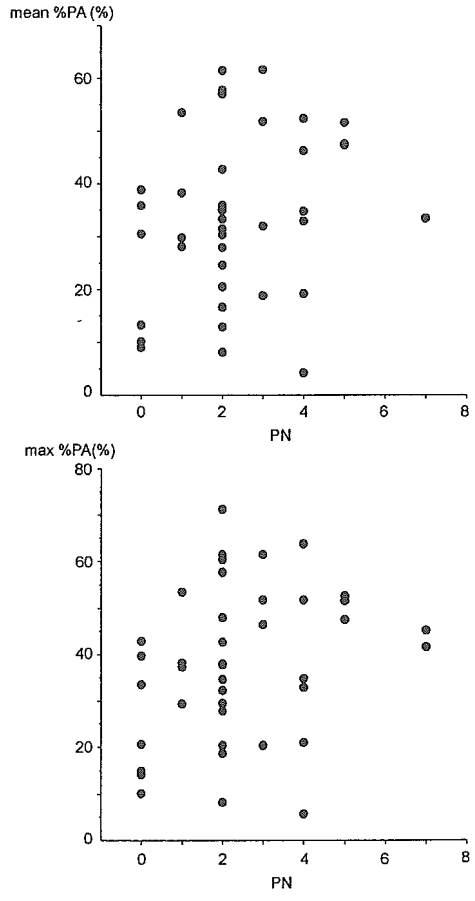

Table 3. All Clinical and Carotid Ultrasonographic Parameters and Relationship With Mean and Maximum Percent Plaque Area in the Multivariate Analysis

Parameter	Mean %PA		Max %PA	
	β	*P*	β	*P*
Male	0.37	.005	0.35	.010
Hypertension	0.46	.003	0.36	.021
Max IMT-C avg	0.50	.006	0.51	.008
PN	−0.24	.21	−0.21	.30

Max IMT-C avg indicates average maximum IMT of each side of the common carotid artery; Max %PA, maximum percent plaque area; Mean %PA, mean percent plaque area; and PN, plaque number.

Discussion

It has been reported that the IMT of the carotid artery is related not only to the presence of CAD but also to the occurrence of coronary events[5–8,19,20] There have been few reports concerning the relationship between carotid and left main coronary artery stenosis in patients undergoing coronary angiography.[21] Coronary angiography significantly underestimates the presence of atherosclerotic stenosis in the left main coronary artery because of coronary remodeling and methodological limitations.[16,22–24] Conversely, because IVUS permits detailed, high-quality cross-sectional imaging of the coronary arteries in vivo, we can evaluate the precise extent of left main coronary artery atherosclerosis. This study showed that the average of the maximum common carotid IMT, a parameter of carotid ultrasonographic findings, was correlated with accurate measurements of left main coronary artery atherosclerosis. It is well known that left main CAD is related to a patient's prognosis. Therefore, this carotid ultrasonographic finding may be associated with long-term prognosis. However, more research is needed on the correlation between the degree of carotid atherosclerosis and long-term prognosis.

A limitation of this study was that all patients had CAD. This selection bias meant that our findings regarding the relationship between carotid disease and left main CAD are relevant only to this specific group of patients and may not be applied to the general population.

Hypercholesterolemia and diabetes mellitus are known as important risk factors for the development of coronary atherosclerosis in Japan. In this study, however, male sex and hypertension were independent predictive factors rather than hypercholesterolemia and diabetes mellitus because all patients had CAD.

In conclusion, left main coronary artery atherosclerosis seems to be correlated with the average of the maximum common carotid IMT assessed by carotid ultrasonography as well as with men and the presence of hypertension. The average of the maximum common carotid IMT is the most important carotid ultrasonographic factor associated with left main coronary artery atherosclerosis.

References

1. Young W, Gofman JW, Tandy R. The quantification of atherosclerosis? The extent of correlation of degrees of atherosclerosis within and between the coronary and cerebral vascular beds. Am J Cardiol 1960; 6:300–308.
2. Mitchell JRA, Schwartz CJ. Relationship between arterial disease in different sites: a study of the aorta and coronary carotid and iliac arteries. Br Med J 1962; 5288:1293–1301.
3. Geroulakos G, O'Gorman D, Nicolaides A, Sheridan D, Elkeles R, Shaper AG. Carotid intima-media thickness: correlation with the British Regional Heart Study risk score. J Intern Med 1994; 235:431–433.
4. Persson J, Formgren J, Israelsson B, Berglund G. Ultrasound-determined intima-media thickness and atherosclerosis: direct and indirect validation. Arterioscler Thromb 1994; 14:261–264.
5. Geroulakos G, O'Gorman DJ, Kalodiki E, Sheridan DJ, Nicolaides AN. The carotid intima-media thickness as a marker of the presence of severe symptomatic coronary artery disease. Eur Heart J 1994; 15:781–785.
6. Crouse JR III, Craven TE, Hagaman AP, Bond MG. Association of coronary disease with segment-specific intimal-medial thickening of the extracranial carotid artery. Circulation 1995; 92:1141–1147.
7. Sugo A, Nakajima S, Kurata T, Mokuno H, Daida H, Yamaguchi H. Ultrasonographic assessment of carotid atherosclerosis emphasizing the variety of intimal-medial thickness and the relationship with coronary risk factors. J Cardiol 1997; 30:321–329.

8. Balbarini A, Buttitta F, Limbruno U, et al. Usefulness of carotid intima-media thickness measurement and peripheral B-mode ultrasound scan in the clinical screening of patients with coronary artery disease. Angiology 2000; 51:269–279.

9. Wofford JL, Kahl FR, Howard GR, McKinney WM, Toole JF, Crouse JR III. Relation of extent of extracranial carotid artery atherosclerosis as measured by B-mode ultrasound to the extent of coronary atherosclerosis. Arterioscler Thromb 1991; 11:1786–1794.

10. Craven TE, Ryu JE, Espeland MA, et al. Evaluation of the associations between carotid artery atherosclerosis and coronary artery stenosis: a case-control study. Circulation 1990; 82:1230–1242.

11. Bruckert E, Giral P, Salloum J, et al. Carotid stenosis is a powerful predictor of a positive exercise electrocardiogram in a large hyperlipidemic population. Atherosclerosis 1992; 92:105–114.

12. Giral P, Bruckert E, Dairou F, et al. Usefulness in predicting coronary artery disease by ultrasonic evaluation of the carotid arteries in asymptomatic hypercholesterolemic patients with positive exercise stress tests. Am J Cardiol 1999; 84:14–17.

13. Conti CR, Selby JH, Christie LG, et al. Left main coronary artery stenosis: clinical spectrum, pathophysiology, and management. Prog Cardiovasc Dis 1979; 22:73–106.

14. Lim JS, Proudfit WL, Sones FM Jr. Left main coronary arterial obstruction: long-term follow-up of 141 nonsurgical cases. Am J Cardiol 1975; 36:131–135.

15. Takaro T, Peduzzi P, Detre KM, et al. Survival in subgroups of patients with left main coronary artery disease: Veterans Administration Cooperative Study of Surgery for Coronary Arterial Occlusive Disease. Circulation 1982; 66:14–22.

16. Ge J, Liu F, Gorge G, Haude M, Baumgart D, Erbel R. Angiographically "silent" plaque in the left main coronary artery detected by intravascular ultrasound. Coron Artery Dis 1995; 6:805–810.

17. Kawano S, Yamagishi M, Hao H, Yutani C, Miyatake K. Wall composition in intravascular ultrasound layered appearance of human coronary artery. Heart Vessels 1996; 11:152–159.

18. Handa N, Matsumoto M, Maeda H, Hougaku H, Kamada T. Ischemic stroke events and carotid atherosclerosis: results of the Osaka Follow-up Study for Ultrasonographic Assessment of Carotid Atherosclerosis (the OSACA Study). Stroke 1995; 26:1781–1786.

19. del Sol AI, Moons KG, Hollander M, et al. Is carotid intima-media thickness useful in cardiovascular disease risk assessment? The Rotterdam Study. Stroke 2001; 32:1532–1538.

20. Hodis HN, Mack WJ, LaBree L, et al. The role of carotid arterial intima-media thickness in predicting clinical coronary events. Ann Intern Med 1998; 128:262–269.

21. Kallikazaros I, Tsioufis C, Sideris S, Stefanadis C, Toutouzas P. Carotid artery disease as a marker for the presence of severe coronary artery disease in patients evaluated for chest pain. Stroke 1999; 30:1002–1007.

22. Yamagishi M, Hongo Y, Goto Y, et al. Intravascular ultrasound evidence of angiographically undetected left main coronary artery disease and associated trauma during interventional procedures. Heart Vessels 1996; 11:262–268.

23. Hermiller JB, Buller CE, Tenaglia AN, et al. Unrecognized left main coronary artery disease in patients undergoing interventional procedures. Am J Cardiol 1993; 71:173–176.

24. Gerber TC, Erbel R, Gorge G, Ge J, Rupprecht HJ, Meyer J. Extent of atherosclerosis and remodeling of the left main coronary artery determined by intravascular ultrasound. Am J Cardiol 1994; 73:666–671.

Neuroradiology (2005) 47: 256–262
DOI 10.1007/s00234-005-1364-x

Toshiyasu Ogata
Kazumi Kimura
Makoto Nakajima
Hiroaki Naritomi
Kazuo Minematsu

Diagnosis of middle cerebral artery occlusive lesions with contrast-enhanced transcranial color-coded real-time sonography in acute stroke

Received: 24 September 2004
Accepted: 8 February 2005
Published online: 24 March 2005

T. Ogata · K. Kimura
M. Nakajima · H. Naritomi
K. Minematsu
Cerebrovascular Division,
Department of Medicine,
National Cardiovascular Center,
Japan

Present address: T. Ogata (✉)
Department of Medicine and Clinical Science, Graduate School of Medical Sciences, Kyushu University,
Maidashi 3-1-1, Higashiku Fukuoka 812-8582, Japan
E-mail:
togata@intmed2.med.kyushu-u.ac.jp
Tel.: +81-92-6425256
Fax: +81-92-6425271

Abstract It is useful to evaluate the occlusive lesions of middle cerebral artery (MCA) occlusion with transcranial color-coded real-time sonography (TCCS). However, TCCS criteria for locating the site of the MCA occlusion has, as yet, remained unclear. The aim of the present study was to establish TCCS criteria for MCA occlusive lesions. We prospectively performed contrast-enhanced TCCS (CE-TCCS) in 75 consecutive acute stroke patients within 24 h of digital subtraction angiography. Patients were divided into four groups: occlusion of the MCA stem (MO group, $n=12$); occlusion of the MCA branch (MBO group, $n=10$); stenosis of the MCA stem (MS group, $n=9$); and no occlusive or stenotic lesions (control group, $n=44$). The following parameters were measured: peak systolic velocity (PSV) and end diastolic velocity (EDV) of bilateral MCA stems, and ED-ratio (the side-to-side ratio of the EDV). We establish the CE-TCCS criteria for MCA occlusive lesions using the sensitivity–specificity curve analysis. A PSV of 170 cm/s distinguished MCA stenosis from other groups (positive and negative predictive values and the accuracies were 100%, 99.0% and 99.1%, respectively). An EDV of 26 cm/s differentiated MO or MBO from the other groups (positive and negative predictive values and the accuracies were 84.6%, 100% and 96.5%, respectively). An ED-ratio of 2.5 discriminated MO from the MBO group (positive and negative predictive values and the accuracies were 88.9%, 85.7% and 87.5%, respectively). Measurement of MCA stem flow velocity with CE-TCCS can identify MCA stem stenosis and occlusion, as well as MCA branch occlusion.

Keywords Acute cerebral infarction · Angiography · Ultrasonography · Doppler · Transcranial · Contrast media

Introduction

In 1982, Aaslid et al. [1] utilized Doppler technology to characterize skull base arterial flow via a temporal window. Since that time, transcranial Doppler (TCD) sonography has been widely used to evaluate various conditions, including intracranial hemodynamic alterations, vasospasm after subarachnoid hemorrhage, intracranial arterial stenosis and occlusion, and arteriovenous malformations [2–7].

In the early 1990s, transcranial color-coded real-time sonography (TCCS) was introduced, which added real-time B-mode imaging and color coding of the Doppler signal to conventional TCD sonography [8–10]. Using this technique, identification of specific vascular structures was increasingly successful when compared with

identification by TCD. TCCS also allowed for measurement of the angle of insonation and determination of absolute velocities with greater precision [11, 12].

The use of contrast enhancement further improved the diagnostic utility of TCCS, even in the face of temporal bone window failure [13–17]. Contrast-enhanced TCCS (CE-TCCS) has subsequently been validated for the identification of occlusive middle cerebral artery (MCA) lesions in patients with ischemic stroke [18, 19].

Several reports have proposed criteria for the detection of MCA occlusion or MCA stenosis with TCCS [19–21]. However, TCCS criteria for MCA branch occlusion have not yet been investigated. We hypothesized that the blood flow velocity in the MCA stem was dependent on the specific site of occlusion and that measurement of the blood flow velocity in the MCA stem may aid in differentiating between anatomical sites of occlusion. Therefore, the goal of the current study was to establish the TCCS criteria for MCA occlusive disease at specific sites.

Methods

We prospectively performed TCCS in consecutive patients with acute stroke who underwent intra-arterial digital subtraction angiography (IA-DSA) between March 1, 2002 and December 31, 2002. When patients were suspected to have the occlusive lesions in main brain arteries, including posterior circulation from their clinical symptoms, informed consent was obtained from patients and/or their families to perform selective cerebral angiographic study. If the patients had ≥75% stenosis in diameter of the intracranial or extracranial internal carotid artery on IA-DSA, the patients were excluded from this study because of the presence of the hemodynamic effects on MCA flow velocity due to those stenotic lesions. The mean interval from stroke onset to IA-DSA studies was 23.7 h. Four cases who were performed IA-DSA within 12 h from the stroke onset were suspected to have a re-opening of the occluded MCA. The TCCS examination was carried out within 24 h before and after IA-DSA study.

Selective IA-DSA was performed using a biplane, high-resolution angiography system (Angio Rex Super-G and DFP-2000A, Toshiba) with a matrix of 1024 × 1024 pixels. A catheter was inserted into the right brachial artery or femoral artery in accordance with the Seldinger method, and was then guided to the cerebral vasculature for diagnostic four-vessel angiography.

On the basis of the angiographic findings, patients were divided into four groups: occlusion of the MCA stem (MO group, $n=12$); occlusion of the MCA branch (MBO group, $n=10$); stenosis of the MCA stem (MS group, $n=9$); and no occlusive or stenotic lesions (control group, $n=44$). The MS group was defined as stenosis greater than 50% in diameter on the DSA findings.

The equipment for TCCS examination consisted of Sonos 5500 unit (Philips Medical Systems, Japan, Tokyo) with a 1.0–3.0 MHz sector scan. The examination was done by an experienced sonographer (Ogata T). Color Doppler images were routinely obtained, with velocity measurements performed at both sides of the MCAs by pulsed Doppler. The subjects were examined first in the left and then in the right lateral decubitus position. Blood velocity and direction were displayed in real time as color signals within a subsector of the black-and-white image through a temporal bone window. Particular care was taken to obtain a long-axis view of the vessel, especially when visualizing the horizontal portion of the MCA, by means of tilting, rotating, or shifting the transducer. Immediately after conventional TCCS, 8 mL of contrast agent (300 mg/mL; Levovist/Schering, Berlin, Germany) was injected within 10 s through the antecubital vein. Range-gated pulsed Doppler imaging, with a sample volume of 1.9 mm, was used to measure the blood flow velocity in the stem of MCA. The sample volume was moved slowly, starting proximally and proceeding distally to the horizontal segment of the MCA and was displayed as color flow imaging on B-mode images. Peak systolic flow velocity (PSV) and the end-diastolic flow velocity (EDV) of both MCAs were measured within 5 min after the contrast agent injection. The mean value of these parameters during five consecutive cardiac cycles was also determined, and absolute velocities were noted, together with correction for the incident angle. Particular care was taken to keep the incident angle between the MCA and the beam at 60° or less. Furthermore, the side-to-side ratio of the EDV (ED-ratio) was calculated by dividing the velocity of the unaffected side by that of the affected side in the MO and MBO groups.

The patients' age and blood flow velocity data were expressed as mean ± SD. One-way factorial ANOVA was used to analyze velocity differences among the four groups. A sensitivity–specificity curve analysis was applied to obtain cutoff values for: (1) PSV for distinguishing MS from other groups; (2) EDV for distinguishing MO or MBO from other groups; and (3) ED-ratio for differentiating MO from the MBO group. A value of $p<0.05$ was accepted as a significant difference.

Results

A total of 75 patients (61 men and 14 women; 64.9 ± 13.0 years old) underwent both IA-DSA and CE-TCCS. PSV and EDV were measured in the MCA(s)

either bilaterally ($n=60$) or unilaterally ($n=15$), yielding assessment of a total of 135 vessels in the present study. Stenotic or occlusive lesions were present in this population, including 12 patients with unilateral MCA occlusion, nine patients with unilateral MCA branch occlusion, one patient with bilateral MCA branch occlusions, seven patients with unilateral MCA stenosis, two patients with bilateral MCA stenosis, and 44 patients without significant stenosis. Thus, the experimental groups consisted of: occlusion of the MCA stem (MO group, $n=12$); occlusion of the MCA branch (MBO group, $n=10$); stenosis of the MCA stem (MS group, $n=9$); and no occlusive or stenotic lesions (control group, $n=44$). No difference in patient demographics (age, gender, frequency of hypertension, diabetes mellitus, smoking history, presence of atrial fibrillation) was present when comparing the four groups. Furthermore, Doppler findings were not different among types of stroke.

Blood flow velocity could not be measured by CE-TCCS in one patient in the MO group and one patient in the MS group because of a lack of blood flow signal. Typical waveforms in the MO, MBO, and MS groups are shown in Fig. 1.

The PSV, EDV, and ED-ratio in each group are shown in Fig. 2. The PSV in the control group was 104.6 ± 26.4 cm/s, with all values less than 170 cm/s. The PSV was significantly higher in the MS group (274.2 ± 110.1 cm/s) when compared with other groups ($p < 0.001$ for Scheffe test).

The EDV of the affected side in the MO and MBO groups was 13.7 ± 4.3 and 22.7 ± 2.1 cm/s, respectively, with all values less than 26 cm/s. EDV was significantly higher in the control group (41.6 ± 12.1 cm/s) when compared with the MO (13.7 ± 4.3 cm/s) or MBO (22.7 ± 2.1 cm/s) groups ($p < 0.001$, vs. MO and $p < 0.05$, vs. MBO, for Scheffe test).

The ED-ratio was not calculated in three patients with bilateral MCA stenosis or occlusion, leaving a

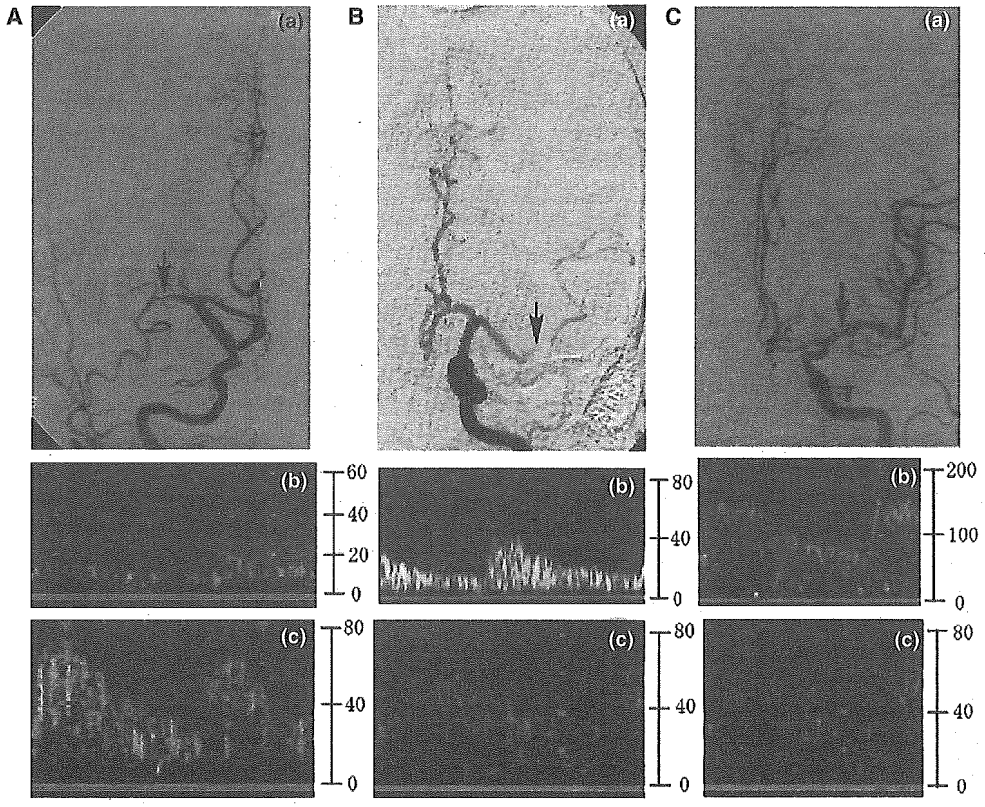

Fig. 1 **A** A representative case of middle cerebral artery (MCA) occlusion evaluated with cerebral angiography and contrast-enhanced transcranial color-coded real-time sonography (CE-TCCS). **a** Right carotid angiogram, anteroposterior view, shows the occlusion of the horizontal portion in the left MCA (*arrow*). **b** Doppler wave forms of the right MCA shows an EDV of 10.8 cm/s. **c** Doppler wave forms of the left MCA shows an EDV of 28.4 cm/s. **B** The CE-TCCS and digital subtraction angiography (DSA) findings in the patient with MCA branch occlusion. **a** Left carotid angiogram, anteroposterior view, shows the occlusion of the branch in the left MCA (*arrow*). **b, c** Doppler wave forms show that the EDV of the occluded side of MCA is 19.9 cm/s, and that of the normal side is 38.2 cm/s. **C** The CE-TCCS and DSA findings of the representative case of MCA stenosis. **a** Left carotid angiogram confirms stenosis of the horizontal portion in the right MCA (*arrow*). **b, c** PSV of left MCA stem is 178 cm/s. PSV of right MCA stem is 73 cm/s

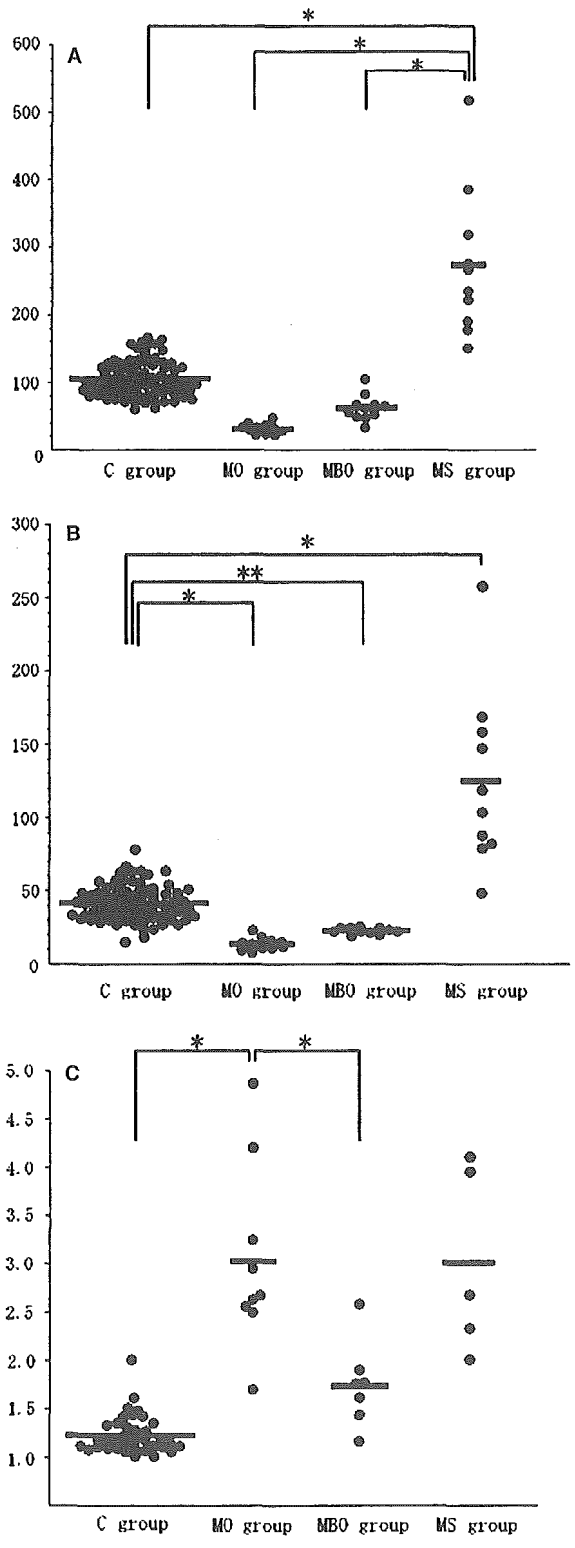

◀

Fig. 2 **a** Scattergram of PSV of occlusion of the MCA stem (MO), occlusion of the MCA branch (MBO), stenosis of the MCA stem (MS), and the control groups. The mean ± 2SD of the PSV of the control, MO, MBO, and MS groups was 104.6 ± 26.4, 31.9 ± 7.8, 62.3 ± 18.9, and 274.2 ± 110.1, respectively. * $p < 0.001$, for Scheffe test. **b** EDV in the MO, MBO, MS, and control groups. The EDV is significantly lower in the MO and MBO groups (13.7 ± 4.3 and 22.7 ± 2.1, respectively) than that in the MS and control groups (41.6 ± 12.1 and 125.6 ± 60.4, respectively). * $p < 0.001$, for Scheffe test. ** $p < 0.05$, for Scheffe test. **c** Comparison of the side-to-side ratio of the end-diastolic flow velocity (ED-ratio) of the MO, MBO, MS, and control groups. The mean ± 2SD of the ED-ratio of the control, MO, MBO, and MS groups was 1.2 ± 0.2, 3.0 ± 1.0, 1.7 ± 0.4, and 3.0 ± 1.0, respectively. * $p < 0.001$, for Scheffe test

total of 57 patients for assessment. The ED-ratio was significantly higher in the MO group than in the MBO group (1.7 ± 0.4 vs. 3.0 ± 1.0, $p < 0.001$, for Scheffe test).

In the sensitivity–specificity curve analysis, the optimal threshold value of PSV for predicting MCA stenosis was 170 cm/s (Fig. 3a). Calculation of positive and negative predictive values and accuracy when using the optimal threshold value of 170 cm/s was 100%, 99.0%, and 99.1%, respectively. The optimal threshold value of EDV for differentiating MO and MBO from the other groups was 26 cm/s (Fig. 3b). Calculation of positive and negative predictive values and accuracy when using the optimal threshold value was 84.6%, 100%, and 96.5%, respectively. The optimal threshold value of ED-ratio for discriminating MO from MBO was 2.5 (Fig. 3c). Calculation of positive and negative predictive values and accuracy when using the optimal threshold value was 88.9%, 85.7%, and 87.5%, respectively.

Discussion

The current data generated by CE-TCCS examination provided objective criteria for the diagnosis of MCA stem stenosis and occlusion, as well as MCA branch occlusion.

TCD sonography has been used to identify occlusion and stenosis of the MCA stem [5–7]. However, the inability for precise sample volume placement and angle insonation makes TCD unsuitable for the measurement of absolute flow velocities. Indeed, Suwanwela et al. [22] reported that TCD could not detect distal MCA stenosis because of technical difficulties. In contrast, TCCS can visualize the horizontal portion of the MCA and measure absolute flow velocity [11, 12]. The utility of TCCS is further enhanced via the use of contrast, thus, yielding more accurate MCA flow velocities when compared with conventional TCD [13, 19–21, 23, 24].

In a previous study using TCD, the diagnosis of MCA occlusion was based on the absence of Doppler signals at a depth of insonation corresponding to the MCA with preservation of anterior and posterior

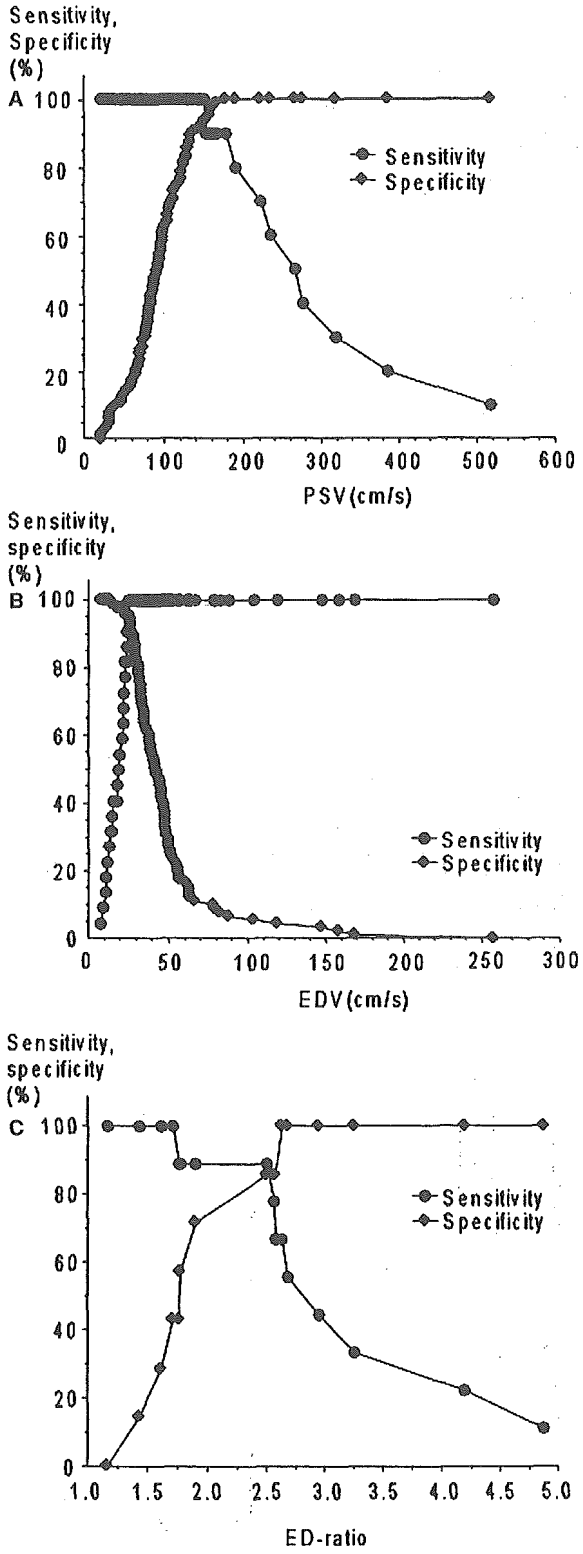

◀

Fig. 3 **a** A sensitivity–specificity curve for predicting MS by PSV. The optimal threshold value of PSV for predicting MS greater than 50% is 170 cm/s. **b** The sensitivity–specificity curve analysis exhibits that the optimal threshold value of EDV for predicting MO and MBO is 26 cm/s. **c** By use of the sensitivity–specificity curve, the optimal threshold value of EDV-ratio for differentiating MO from MBO is shown to be 2.5

cerebral artery signals [5]. Kimura et al. [20] reported that conventional TCCS could detect MCA flow velocity of the distal MCA stem occluded side and that the ED-ratio was greater than 1.9. However, criteria for the diagnosis of MCA branch occlusion by TCCS or CE-TCCS have not been reported. Because flow velocity in the MCA branches is slower than that in the MCA stem and the angle that the branches subtend to the ultrasound probe is increased [19], it is not always possible to visualize the MCA branches using TCCS. Therefore, we used the flow velocity in the MCA stem to evaluate MCA branch occlusion as well as MCA stem occlusion.

The diagnostic algorithm for MCA stem and branch occlusion and MCA stem stenosis is shown in Fig. 4. By using this algorithm, we could accurately diagnose 90% of the patients in our population.

One of the limitations of TCCS is the suitability of the acoustic window, particularly in elderly women [16]. Recent reports indicated that contrast enhancement improves the diagnostic potential of TCCS significantly in patients with temporal bone window failure [13–17]. Although we used contrast agents in this study, we could not detect the basal cerebral arteries of some patients. The detection rate of the intracranial artery flow signal using TCD is lower in Japanese patients than in Caucasian patients [25]. Future technical innovations may reduce these limitations.

TCCS equipment is portable and, therefore, can be used at the bedside. TCCS can be performed rapidly because the cerebral vessels can be imaged within 1 min, provided an adequate acoustic window is achieved. Furthermore, the measurement of MCA flow velocity by the Sonos 5500 unit is well catered for by other equipment. Because of these qualities, TCCS can be repeated easily and may be useful in monitoring the clinical response to therapeutic intervention.

In conclusion, we demonstrated that the assessment of the MCA flow velocity by TCCS could diagnose and distinguish between MCA stem and branch occlusion and stenosis in the MCA stem. TCCS is a useful tool in the assessment of acute stroke patients.

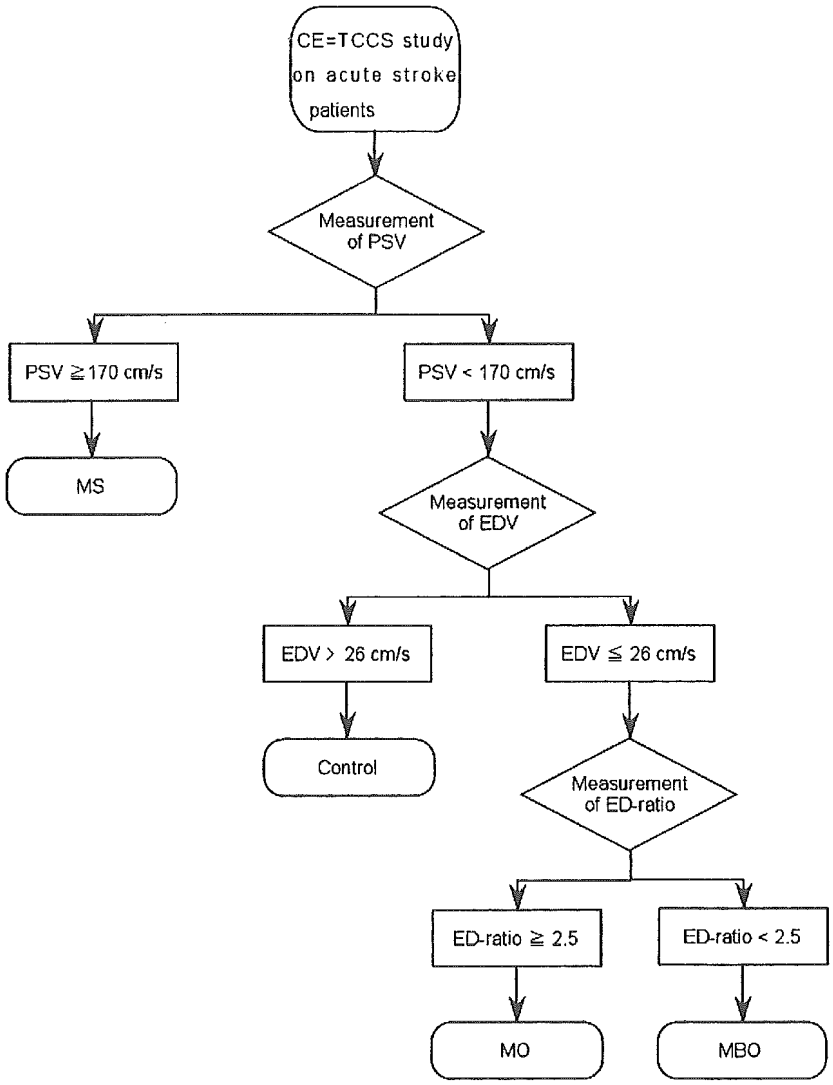

Fig. 4 Algorithm for diagnosing MO, MBO, and MS using PSV, EDV, and ED-ratio of CE-TCCS

References

1. Aaslid R, Markwalder TM, Nornes H (1982) Noninvasive transcranial Doppler ultrasound recording of flow velocity in basal cerebral arteries. J Neurosurg 57:769–774
2. Lindegaard KF, Bakke SJ, Grolimund P, Aaslid R, Huber P, Nornes H (1985) Assessment of intracranial hemodynamics in carotid artery disease by transcranial Doppler ultrasound. J Neurosurg 63:890–898
3. Aaslid R, Huber P, Nornes H (1984) Evaluation of cerebrovascular spasm with transcranial Doppler ultrasound. J Neurosurg 60:37–41
4. Wechsler LR, Ropper AH, Kistler JP (1986) Transcranial Doppler in cerebrovascular disease. Stroke 17:905–912
5. Ley-Pozo J, Ringelstein EB (1990) Noninvasive detection of occlusive disease of the carotid siphon and middle cerebral artery. Ann Neurol 28:640–647
6. Lindegaard KF, Bakke SJ, Aaslid R, Nornes H (1986) Doppler diagnosis of intracranial artery occlusive disorders. J Neurol Neurosurg Psychiatry 49:510–518
7. Mattle H, Grolimund P, Huber P, Sturzenegger M, Zurbrugg HR (1988) Transcranial Doppler sonographic findings in middle cerebral artery disease. Arch Neurol 45:289–295
8. Bogdahn U, Becker G, Winkler J, Greiner K, Perez J, Meurers B (1990) Transcranial color-coded real-time sonography in adults. Stroke 21:1680–1688
9. Martin PJ, Evans DH, Naylor AR (1994) Transcranial color-coded sonography of the basal cerebral circulation. Reference data from 115 volunteers. Stroke 25:390–396
10. Tsuchiya T, Yasaka M, Yamaguchi T, Kimura K, Omae T (1991) Imaging of the basal cerebral arteries and measurement of blood velocity in adults by using transcranial real-time color flow Doppler sonography. Am J Neuroradiol 12:497–502
11. Martin PJ, Evans DH, Naylor AR (1995) Measurement of blood flow velocity in the basal cerebral circulation: advantages of transcranial color-coded sonography over conventional transcranial Doppler. J Clin Ultrasound 23:21–26

12. Klotzsch C, Popescu O, Sliwka U, Mull M, Noth J (2000) Detection of stenoses in the anterior circulation using frequency-based transcranial color-coded sonography. Ultrasound Med Biol 26:579–584
13. Goertler M, Kross R, Baeumer M, Jost S, Grote R, Weber S, Wallesch CW (1998) Diagnostic impact and prognostic relevance of early contrast-enhanced transcranial color-coded duplex sonography in acute stroke. Stroke 29:955–962
14. Baumgartner RW, Arnold M, Gonner F, Staikow I, Herrmann C, Rivoir A, Muri RM (1997) Contrast-enhanced transcranial color-coded duplex sonography in ischemic cerebrovascular disease. Stroke 28:2473–2478
15. Zunker P, Wilms H, Brossmann J, Georgiadis D, Weber S, Deuschl G (2002) Echo contrast-enhanced transcranial ultrasound: frequency of use, diagnostic benefit, and validity of results compared with MRA. Stroke 33:2600–2603
16. Postert T, Braun B, Meves S, Koster O, Przuntek H, Weber S, Buttner T (1999) Contrast-enhanced transcranial color-coded sonography in acute hemispheric brain infarction. Stroke 30:1819–1826
17. Gerriets T, Seidel G, Fiss I, Modrau B, Kaps M (1999) Contrast-enhanced transcranial color-coded duplex sonography: efficiency and validity. Neurology 52:1133–1137
18. Gerriets T, Goertler M, Stolz E, Postert T, Sliwka U, Schlachetzki F, Seidel G, Weber S, Kaps M (2002) Feasibility and validity of transcranial duplex sonography in patients with acute stroke. J Neurol Neurosurg Psychiatry 73:17–20
19. Kenton AR, Martin PJ, Abbott RJ, Moody AR (1997) Comparison of transcranial color-coded sonography and magnetic resonance angiography in acute stroke. Stroke 28:1601–1606
20. Kimura K, Hashimoto Y, Hirano T, Uchino M, Ando M (1996) Diagnosis of middle cerebral artery occlusion with transcranial color-coded real-time sonography. Am J Neuroradiol 17:895–899
21. Kimura K, Yasaka M, Wada K, Minematsu K, Yamaguchi T, Otsubo R (1998) Diagnosis of middle cerebral artery stenosis by transcranial color-coded real-time sonography. Am J Neuroradiol 19:1893–1896
22. Suwanwela NC, Phanthumchinda K, Suwanwela N (2002) Transcranial Doppler sonography and CT angiography in patients with atherothrombotic middle cerebral artery stroke. Am J Neuroradiol 23:1352–1355
23. Wada K, Kimura K, Minematsu K, Yasaka M, Uchino M, Yamaguchi T (2002) Combined carotid and transcranial color-coded sonography in acute ischemic stroke. Eur J Ultrasound 15:101–108
24. Seidel G, Kaps M, Gerriets T (1995) Potential and limitations of transcranial color-coded sonography in stroke patients. Stroke 26:2061–2066
25. Itoh T, Matsumoto M, Handa N, Maeda H, Hougaku H, Hashimoto H, Etani H, Tsukamoto Y, Kamada T (1993) Rate of successful recording of blood flow signals in the middle cerebral artery using transcranial Doppler sonography. Stroke 24:1192–1195

Highly Diffusion-Sensitized Tensor Imaging of Unilateral Cerebral Arterial Occlusive Disease

Atsushi Shiraishi, Yasuhiro Hasegawa, Shunichi Okada, Kazumi Kimura, Tohru Sawada, Hidehiro Mizusawa, and Kazuo Minematsu

BACKGROUND AND PURPOSE: **Selective neuronal death is a well-recognized histopathologic sequel to moderate ischemic brain damage. However, radiologic visualization of these changes has not been established, even with diffusion tensor imaging (DTI). We sought to determine whether DTI with *b* values ≥1900 s/mm^2 reveals occult diffusion abnormalities in patients with cerebral arterial occlusive disease.**

METHODS: **Six patients (five men, one woman; mean age ± standard deviation, 66 ± 8 years) with unilateral internal carotid or middle cerebral arterial occlusive disease but not parenchymal T2 hyperintensity underwent 3T fast DTI with $b \leq 1300$ s/mm^2 and slow DTI with $b \geq 1900$ s/mm^2. We postprocessed mean diffusibility and fractional anisotropy (FA) images from the fast and slow DTI datasets. Standardized asymmetry indices (AIs) were used to identify regional asymmetries. Diagnostic accuracy among the DTI modalities was assessed by means of receiver operating characteristic analysis.**

RESULTS: **In hemispheres ipsilateral to occluded vessel, AIs were significantly elevated on fast mean-diffusibility images of white matter at the levels of the internal capsule (95% confidence interval [CI]: 1.00, 1.09; $P = .045$) and corona radiata (95% CI: 1.01, 1.12; $P = .034$). AIs were significantly decreased on slow FA images at the internal capsule (95% CI: 0.84, 0.98; $P = .018$) and white matter at the internal capsule level (95% CI: 0.92, 1.00, $P = .043$). The slow FA map had the highest accuracy (89.8%) for detecting the hemisphere ipsilateral to arterial occlusion.**

CONCLUSION: **Slow FA maps acquired by using DTI with high *b* values are useful for visualizing ischemic brain damage in apparently normal WM.**

Selective neuronal death is well recognized as a histopathologic sequel of ischemic brain damage less severe than infarction (1–5). Selective neuronal death reveals regional loss of limited number of neurons without coagulation necrosis or cavitation of the neural tissue. Several histopathologic studies have demonstrated selective neuronal death in experimental animals (1–4) and human autopsy cases (5) with ischemic insults.

By using conventional MR imaging, brain infarction was widely accepted as depression of the apparent diffusion coefficient (ADC) with acute brain ischemia and T2 hyperintensities; however, radiologic visualization of selective neuronal death remains limited. Only studies of *in vivo* benzodiazepine receptor mapping (6, 7) or magnetization transfer imaging (8) in patients with acute (6) or chronic nonfatal ischemia (7, 8) have supported this concept for selective neuronal death.

Progress in diffusion MR imaging has advanced the immediate diagnosis of hyperacute ischemic stroke. Furthermore, applications of diffusion MR imaging continue to expand from the estimation of diffusion amplitudes, which enables the diagnosis of stroke on diffusion-weighted imaging (DWI), to the estimation of complete diffusion tensor, which may improved resolution of white matter (WM) microstructures in both healthy and diseased conditions on diffusion tensor imaging (DTI). DTI depicts tissue diffusion characteristics as 3D ellipsoids (9). Postprocessed from these ellipsoids, DTI maps can reveal both amplitudes and anisotropy indexes of tissue diffusion properties on a voxel-by-voxel basis.

Received August 13, 2004; accepted after revision November 24.

From the Cerebrovascular Division, National Cardiovascular Center (A.S., Y.H., S.O., K.K., K.M.), and the BF Research Institute (T.S.), Osaka, and the Department of Neurology and Neurological Science, Graduate School of Medical and Dental Science, Tokyo Medical and Dental University (A.S., H.M.), Japan.

Supported in part by a Research Grant for Cardiovascular Diseases (15C-1) from the Ministry of Health, Labor, and Welfare of Japan.

Address reprint requests to Atsushi Shiraishi, MD, Department of Neurology, Toride Kyodo General Hospital, Hongo 2-1-1, Toride, Ibaraki, 302-0022 Japan.

TABLE 1: Patient demographics

Patient/Age (y)/Sex	Hypertension	Diabetes	Hyperlipidemia	Affected Vessel	Stroke Episode	Time (mo) to Imaging	
						From Diagnosis	From Symptoms
1/68/M	Yes	Yes	Yes	L ICA stenosis	TIA, aphasia	48	4
2/61/M	Yes	Yes	Yes	L MCA stenosis	TIA, dysarthria	21	21
3/55/M	Yes	No	Yes	R ICA occlusion	NA	130	NA
4/66/F	Yes	Yes	Yes	L MCA stenosis	TIA, dysarthria	17	17
5/70/M	Yes	Yes	No	R ICA stenosis	NA	4	NA
6/78/M	Yes	Yes	Yes	L ICA stenosis	NA	3	NA

Note.—NA = not applicable, TIA = transient ischemic attack

DTI with conventional *b* values of ≤1000 s/mm^2 is already accepted as a tool with sufficient sensitivity to depict brain pathologies hidden in normal-appearing WM (10–20). However, in the evaluation of chronic brain ischemia, the sensitivity of DTI is limited because it shows only diffusion abnormalities that coexist with diffuse T2 hyperintensity (12, 18, 21) or secondary neuronal degeneration after stroke (15).

We hypothesized that increased diffusion weighting can reveal the slow-diffusing water component of neural tissue (22–24), which might clarify the subtle WM structural changes that accompanies selective neuronal death. We therefore used DTI with low and high *b* values to evaluate patients with cerebral arterial occlusive disease and minimal T2 changes.

Methods

Patients

The study was approved by the institutional review boards of our institution. To assess the subtle structural changes in the WM independent of apparent lesions, we included only patients with occlusive lesions (≥75% stenosis) of the internal carotid artery (ICA) or middle cerebral artery (MCA). Patients with neurologic deficits were excluded, as were those with any other brain disease, and patients whose most recent neurologic episode occurred <3 months before the study.

We excluded patients with the following findings on fluid-attenuating inversion recovery images (1.5 T, fast spin-echo, TR/TE/TI = 10,000/100/2500, echo train length = 8): apparent symptomatic brain lesions, grade 2 or 3 hyperintensities in the deep WM or periventricular hyperintensities according to the Fazekas scale (25), asymptomatic cortical lesions, or lacunae larger than 3 mm in diameter.

Because of concerns about the safety of high-field-strength MR imaging, patients with implanted metals or medical devices, tattoos, or claustrophobia were excluded. Six patients hospitalized at National Cardiovascular Center, Osaka, Japan, between November 2001 and November 2003 met the study criteria (Table 1). These patients underwent imaging after informed consent was obtained. We also examined six nonage-matched healthy volunteers (three men, three women; mean age ± standard deviation, 29 ± 4 years) after obtaining informed consent and verifying the absence of safety concerns related to MR imaging.

Physiologic Basis of DTI with High b *Values*

The strength of diffusion weighting is quantified by the *b* value (26). For typical *b* values of ≤1000 s/mm^2, diffusional signal-intensity decays can be simply approximated by using the single exponential model (27, 28). However, diffusion MR imaging studies with increased *b* values have revealed that this model is no longer best for describing diffusional signal-intensity decay in the human brain. The decay (S_b/S_0) is better described by the double exponential model, as follows (22–24): $S_b/S_0 = F_{fast} \exp(-D_{fast} \times b) + F_{slow} \exp(-D_{slow} \times b)$, where S_b is the signal intensity with diffusion weighting of the specified *b* value, S_0 is the signal intensity without diffusion weighting, F_{fast} and F_{slow} are the volume fractions of the respective fast and slow components, and D_{fast} and D_{slow} are the ADCs of the respective fast and slow components.

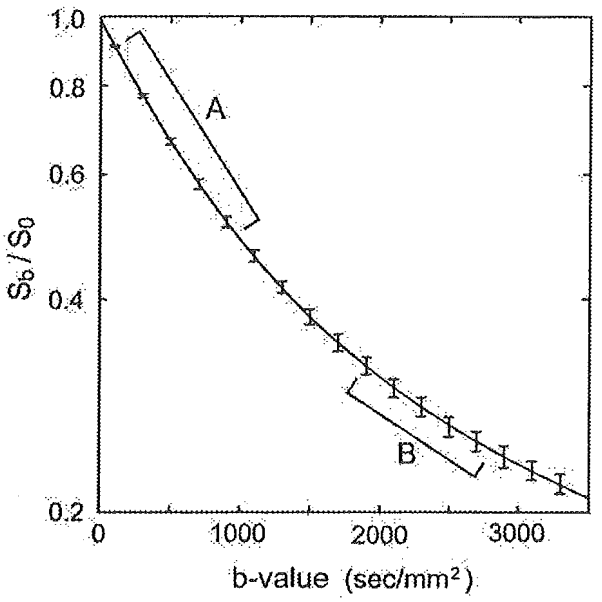

FIG 1. Double-exponential diffusional signal-intensity decays. Plot shows 1) the mean ± 1 SD (*error bars*) of S_b/S_0 at *b* = 100–3300 s/mm^2 in the centrum semiovale in six healthy volunteers and 2) the approximation to the double-exponential model according to the nonlinear least-squares Marquardt–Levenberg algorithm (*line*) plotted on a logarithmic scale. Also shown are *b*-value ranges for fast (*A*) and slow (*B*) DTI in patients 3–6.

Fast components consist of loosely diffusion-restricted water components, which, with differences in *D*, show increased decay with *b*-value increments. Similarly, slow components are tightly diffusion-restricted water components and, as *D* changes, show decreased decay with change in the *b* value. Diffusion MR imaging with low *b* values represents both the fast and slow components; in contrast, imaging with high *b* values dominantly represents the slow diffusion components in eliminating signals from the fast components. To optimize the appropriate use of high *b* values for the slow components, we examined the diffusional signal-intensity decay of six healthy volunteers before beginning the study (Fig 1); these data indicated that we should use *b* values of ≥1900 s/mm^2 to estimate the slow components.

TABLE 2: ROI statistics

	ROI value			Asymmetry Analysis	
	Affected Hemisphere	Unaffected Hemisphere	*P* Value	Standardized AI	*P* Value
Fast MD (10^{-3} sec/mm^2)					
IC	0.67 ± 0.03	0.67 ± 0.03	860	1.00 (0.96–1.04)	882
WM-IC	0.76 ± 0.04	0.73 ± 0.04	071	1.05 (1.00–1.09)	045†
WM-CR	0.78 ± 0.06	0.73 ± 0.03	054	1.06 (1.01–1.12)	034†
WM-CS	0.73 ± 0.03	0.72 ± 0.04	595	1.01 (0.97–1.06)	569
Slow MD (10^{-3} sec/mm^2)					
IC	0.30 ± 0.03	0.28 ± 0.04	168	1.09 (0.98–1.20)	126
WM-IC	0.33 ± 0.04	0.32 ± 0.03	419	1.01 (0.98–1.03)	655
WM-CR	0.32 ± 0.03	0.31 ± 0.02	107	1.02 (0.99–1.04)	128
WM-CS	0.31 ± 0.02	0.31 ± 0.02	473	0.98 (0.95–1.01)	316
Fast FA					
IC	0.65 ± 0.06	0.66 ± 0.05	421	0.98 (0.94–1.01)	194
WM-IC	0.42 ± 0.05	0.44 ± 0.05	142	0.95 (0.89–1.01)	179
WM-CR	0.38 ± 0.05	0.40 ± 0.03	416	0.95 (0.89–1.02)	328
WM-CS	0.37 ± 0.04	0.40 ± 0.02	151	0.94 (0.86–1.01)	112
Slow FA					
IC	0.67 ± 0.08	0.74 ± 0.10	045‡	0.91 (0.84–0.98)	018†
WM-IC	0.58 ± 0.10	0.61 ± 0.08	051	0.96 (0.92–1.00)	043†
WM-CR	0.55 ± 0.09	0.57 ± 0.07	137	0.96 (0.92–1.01)	108
WM-CS	0.54 ± 0.10	0.55 ± 0.09	483	0.98 (0.90–1.05)	545

* Data in parentheses are th 95% CIs.

† Significant.

‡ Significant (paired *t* test).

DTI Parameters

Spin-echo echo-planar imaging that was diffusion-sensitized with six non-colinear motion-probing gradients (9) was implemented on 3.0-T MR imaging systems equipped with gradients of ≤40 mTm^{-1} (Signa Horizon 3.0LX; GE Medical Systems, Milwaukee, WI). We performed the following sequences same section orientation: spin-echo echo-planar T2-weighted imaging, fast DTI with a subset of low *b* values (100, 700, and 1300 s/mm^2 for patients 1 and 2 and 100, 400, 700, and 1000 s/mm^2 for patients 3–6 and control subjects), and slow DTI with a subset of high *b* values (1900, 2500, and 3100 s/mm^2 for patients 1 and 2 and 1900, 2200, 2500, and 2800 s/mm^2 for patients 3–6 and control subjects).

To achieve similar signal intensity-to-noise ratios, we averaged two images for fast DTI and eight images for slow DTI. Total examination times were 41 minutes for patients 1 and 2 and 56 minutes for patients 3–6 and control subjects. Other parameters consisted were a TR/TE of 11500/93.3 ms, a FOV of 220 mm × 220 mm, a matrix of 256 × 256, 16 near-axial sections with 7-mm thickness for patients 1 and 2 or 18 sections with 6-mm thickness for patients 3–6 and control subjects, 100 phase encoding steps, and 256 frequency-encoding steps.

Postprocessing

DTI datasets were automatically corrected for imaging distortions and coregistered in reference to echo-planar T2-weighted image by using software (Statistical Parametric Mapping 2; Functional Imaging Laboratory, Department of Imaging Neuroscience, Institute of Neurology, University College London, UK). These were postprocessed by using image-analysis software (MRVison 1.6.5; MRVision Co., Winchester, MA). Fast and slow tensors were constituted from the respective ADC datasets. Mean diffusibility (MD) and fractional anisotropy (FA) DTI maps (27, 28) were estimated from the fast (for fast MD and FA) and slow (for slow MD and FA) tensor datasets.

Region-of-Interest Analysis

One author (A.S.) semiautomatically defined the polygonal regions of interest (ROIs) to dissect the target WM by using the region-growing method (automatic function) with local thresholding (manual function) on image-analysis software (Osiris 4.1.8; Unite d'Imagerie Numerique, University Hospital of Geneva, Switzerland). ROIs for the internal capsule and those for all of the unilateral WM at sections including the internal capsule (WM-IC), corona radiata (WM-CR), and centrum semiovale (WM-CS) were dissected in reference to fast FA and slow MD images. Each ROI value was quantified simultaneously on all DTIs.

Statistical Analysis

Absolute ROI values of the hemisphere ipsilateral to the arterial occlusion (affected hemisphere) were compared with those of the contralateral (unaffected) hemisphere by using paired *t* tests (Table 2). An asymmetry index (AI) was used for the numerical evaluation of relative changes in ROIs in the affected hemisphere. The AI was calculated by obtaining the ipsilateral-to-contralateral ratio of values in ROI symmetrically placed on axial images. Diffusion characteristics in the normal brain are somewhat asymmetrical (29). Therefore, when the affected hemisphere was on the left, the AI was standardized by being divided by the mean value of the left-to-right ratios of similar ROIs obtained from control subjects. The 95% confidence intervals (CIs) of the standardized AIs were calculated and statistically analyzed (Table 2).

We assessed the diagnostic accuracy of the different DTI modalities in depicting the affected hemisphere by means of receiver operating characteristic (ROC) analysis (Fig 2). A true-positive finding was defined when the individual AI for the affected hemisphere exceeded the threshold for MD or when it was less than the threshold for FA. False-positive findings were similar results in the unaffected hemisphere.

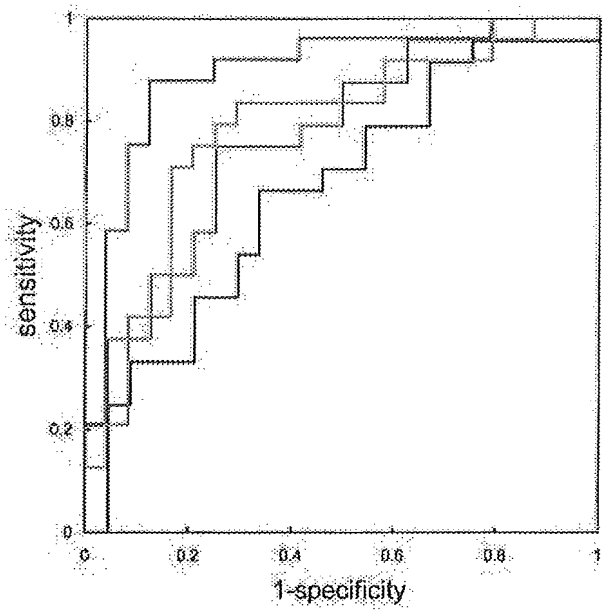

FIG 2. ROC curves for fast MD (*green*), slow MD (*black*), fast FA (*red*), and slow FA (*blue*) indicate estimated accuracies of 78.1% , 69.3%, 77.4%, and 89.8%, respectively. Accuracy of predicting the affected hemisphere was superior for MD on fast DTI and for FA on slow DTI.

Results

Comparison of absolute ROI values demonstrated significant declines in slow FA at the internal capsule of the affected hemisphere (0.74 ± 0.10 vs 0.67 ± 0.08, $P = .045$). We found no significant differences in other ROI values on the slow FA map or in any ROI value on the fast MD, slow MD, or fast FA maps (Table 2). Standardized AIs of the slow FA map showed significant decreases in the internal capsule (95% CI: 0.84, 0.98; $P = .018$) and WM-IC (95% CI: 0.92,1.00; $P = .043$). Standardized AIs on the fast MD maps also showed slight but significant elevations in the WM-IC (95% CI: 1.00, 1.09; $P = .045$) and WM-CR (95% CI: 1.01, 1.12; $P = .034$). ROC analysis showed that the accuracy of detecting the affected hemisphere was 78.1% for fast MD, 69.3% for slow MD, 77.4% for fast FA, and 89.8% for slow FA (Fig 2). Figure 3 shows three sections from the DTI maps in patient 3, who had occlusion of the right internal capsule, and Figure 4 shows sections in patient 4, who had severe stenosis of the left MCA.

Discussion

Tissue diffusion properties can be assessed by means of two postprocessed indices: MD (or ADC) and FA (27, 28). MD represents the magnitude of the diffusion tensor (27, 28), whereas FA represents the shape of the diffusion tensor (28), where an FA of 0 indicates a globular tensor and an FA of 1 indicates a linear tensor. Elevated FA values are probably related to tight diffusion barriers orthogonal to directions of the neural fibers, such as increased attenuation, decreased diameter, and tighter myelination, among others. Declines in FA may indicate neuronal loss, gliosis, and demyelination found in association with various neurologic disorders in normal-appearing WM (10, 11, 13–19).

The proved sensitivity of DTI with conventional b values for the evaluation of various brain pathologies (10, 11, 13, 14, 16, 17, 19, 20) cannot simply be applied to brain ischemia. Previous DTI studies ($b \leq 1000$ s/mm^2) of obstructive cerebrovascular disease (12, 15, 18, 21) have demonstrated MD elevation and anisotropy decline in areas with T2 hyperintensity (12, 15, 18, 21), MD elevation in the normal-appearing WM adjacent to T2 hyperintensity (12, 18), and MD elevation and FA declines in the pyramidal tracts with ipsilateral hemiplegia (15).

Increased diffusion weighting may improve this insensitivity. Clark et al advocated a theoretical framework for the assignment of fast and slow components to extracellular and intracellular fluid (30). Yoshiura et al demonstrated the usefulness of DWI with high b values for the detection of WM degeneration associated with Alzheimer disease (31). In light of these findings, DTI with a high b value might directly reveal the cellular structure, primarily with the slow component, and thereby enable resolution of subtle ischemic changes associated with unilateral cerebral arterial occlusive disease.

We observed changes in the diffusion characteristics of affected hemispheres with minimal abnormalities on fluid-attenuating inversion recovery images. These changes were characterized as elevations in fast rather than slow MD and declines in slow rather than fast FA. ROC analysis indicated that the slow FA map had the best diagnostic accuracy in the affected hemisphere. To our knowledge, ours is the first study to demonstrate changes in properties of the slow component during disease conditions.

Regarding the equation for the double exponential model—$S_b/S_0 = F_{fast} \exp(-D_{fast} \times b) + F_{slow} \exp(-D_{slow} \times b)$—the overall diffusion components represented in the first and second term on the right reflect the fast MD and FA, and the second term represented slow MD and FA that predominantly reflects the slow diffusion component. A possible interpretation of the elevation in fast MD without changes in slow MD is water displacement from the slow to fast component. The changes in MD imply increased loss of the cellular component and its displacement to extracellular fluid, in light of the framework for assignment of fast and slow tensors to extracellular and intracellular fluid (30).

Fast FA can be regarded as a marker of anisotropy for overall diffusion components, including the isotropic and loosely diffusion-restricted extracellular fluid components. In contrast, slow FA is theoretically a marker of anisotropy that predominantly represents the more tightly diffusion-restricted water component. In our study, the slow FA decline independent of changes in fast FA might explain the decreases in the highly anisotropic and tightly diffusion-restricted components.

The histopathologic concept of selective neuronal death is defined as the loss of a limited number of

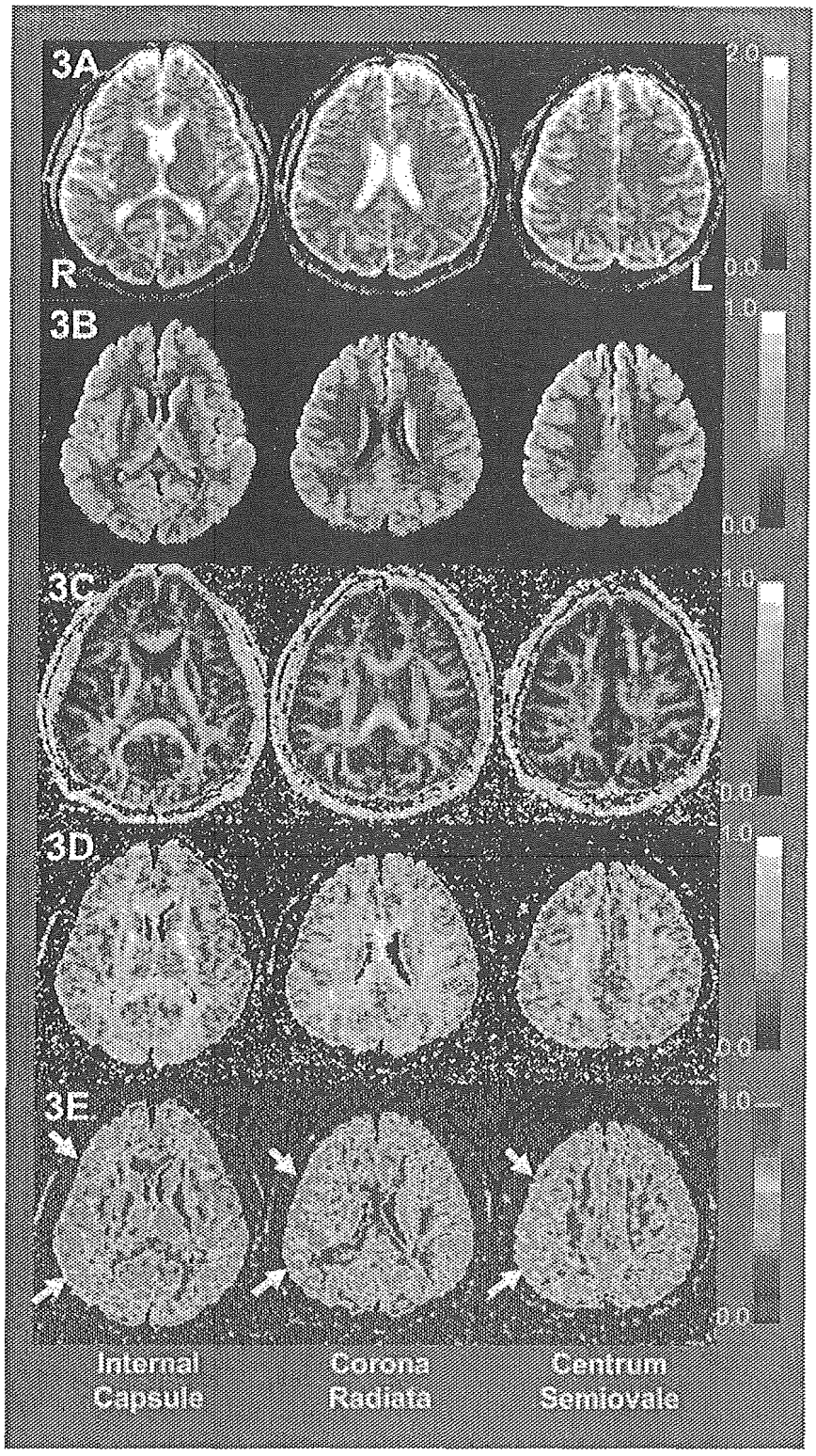

FIG 3. DTIs of patient 3 with right ICA occlusion: fast MD (*3A*), slow MD (*3B*), fast FA (*3C*), slow FA (*3D*), and color-scaled slow FA maps (*3E*) of MD (10^{-3} s/mm^2) and FA. *Arrows* indicate affected hemispheres. In the absence of apparent T2 hyperintensities, the slow FA map of patient 3 demonstrated slight anisotropy declines at right internal capsule.

neurons without coagulation necrosis or cavitation after ischemic insult (1–5); selective neuronal death has been observed in humans (5) and experimental animals (1–4). As *in vivo* radiologic evidence of selective neuronal loss, hypofixation of iodine-123 iomazenil, a surrogate marker of benzodiazepine receptor or neuronal attenuation, was observed in the reperfused gray matter lacking T2 hyperintensity in patients with acute ischemic stroke (6). Data from radiologic studies suggest that chronic but nonfatal brain ischemia may cause selective neuronal death. Yamauchi et al described similar hypofixation of ^{123}I iomazenil in the apparently normal gray matter of chronic brain ischemia (7). As for the WM, Kado et al used magnetization transfer imaging to examine patients with ipsilateral brain ischemia but without ap-

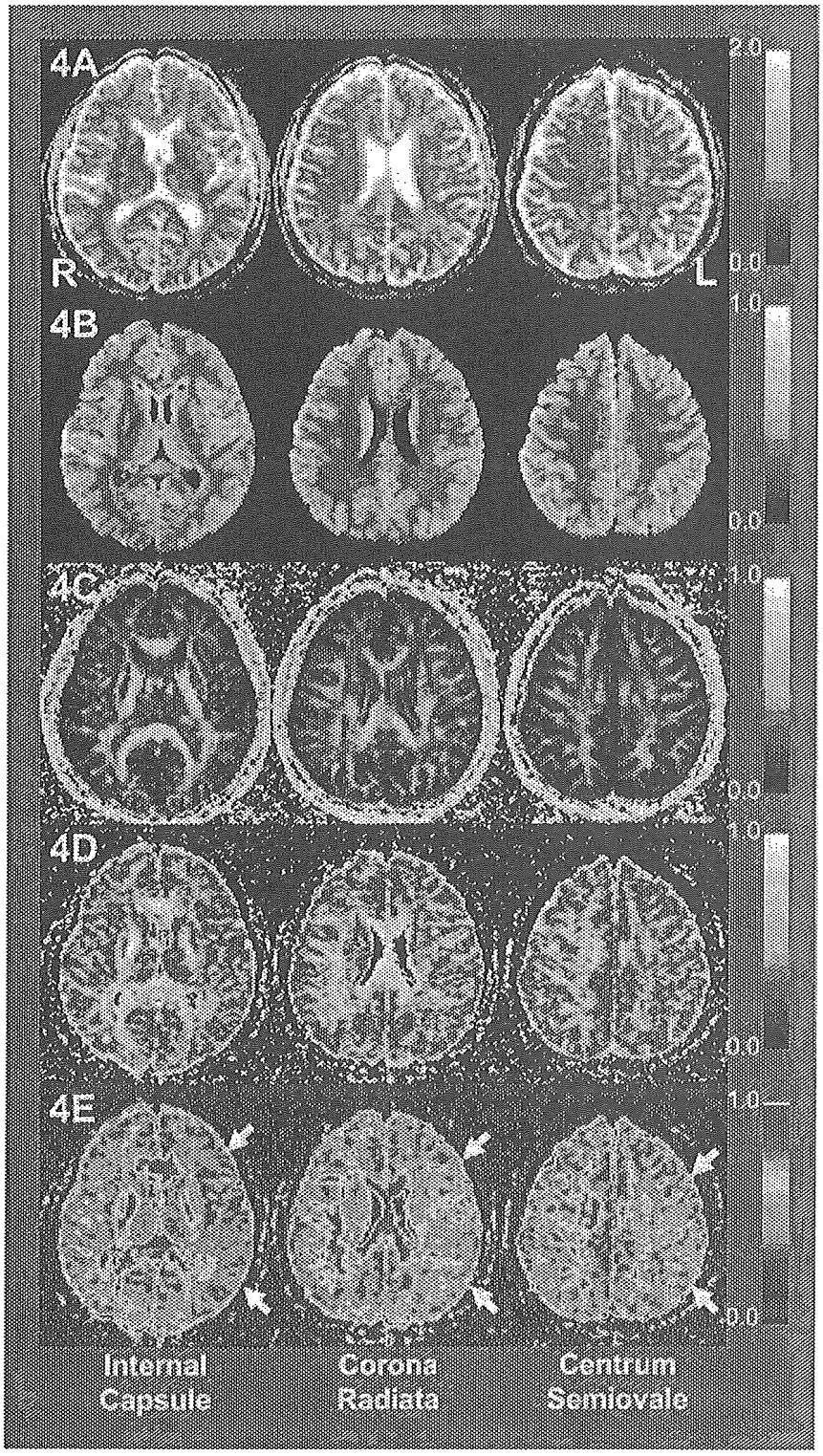

FIG 4. DTIs of patient 4 with left MCA stenosis: fast MD (*4A*), slow MD (*4B*), fast FA (*4C*), slow FA (*4D*). Slow FA map shows broad anisotropy declines in the left hemisphere at all levels shown.

parent T2 hyperintensity; the results suggested changes in the amount and constitution of the myelin present and demonstrated declines in the magnetization transfer ratio and strong linear correlations between the ratio and the cerebral metabolic rate of $oxygen_2$ measured in PET studies (8). Results of these two studies suggest the existence of subtle changes that are broader than the extent of T2 hyperintensity in patients with chronic brain ischemia. Additional changes were inferred from the biophysiologic principles of the radiologic examinations, such as the loss of neurons or myelin content without an increase in the tissue free-water content. Our results indicate decreases in the highly anisotropic slow diffusing component and increases in the fast component. These findings can be interpreted as a loss of axons and myelin content, which contribute to tight diffusion barriers orthogonal to the direction of neural

fibers. In light of these results, loss of neurons (axons) and myelination may occur in the WM ipsilateral to an arterial occlusion that is less severe than infarction. Studies in animal models of chronic brain ischemia (32, 33) indicated the WM pathologies, such as disruption of blood-brain barriers (32), axonal loss (33), and demyelination (33). However, similar pathologic changes in human WM are largely unknown.

A limitation of our study was the lack in histopathologic–radiologic correlation. Future pathologic verification in human studies larger than ours is required.

Conclusion

Slow component DTI with high *b* values may detect occult parenchymal changes in the WM ipsilateral to cerebral arterial occlusive disease.

Acknowledgments

The authors thank Yoshiaki Someya, Seishi Itoi, and Noriko Inoue for their technical support.

References

1. Lassen NA. **Incomplete cerebral infarction: focal incomplete ischemic tissue necrosis not leading to emollision.** *Stroke* 1982;13:522–523
2. Kirino T, Tamura A, Sano K. **Delayed neuronal death in rat hippocampus following transient forebrain ischemia.** *Acta Neuropathol (Berl)* 1984;64:139–147
3. Garcia JH, Lassen NA, Weiller C, Sperling B, Nakagawara J. **Ischemic stroke and incomplete infarction.** *Stroke* 1996;27:761–765
4. Garcia JH, Liu KF, Ye ZR, Gutierrez JA. **Incomplete infarct and delayed neuronal death after transient middle cerebral artery occlusion in rats.** *Stroke* 1997;28:2303–2323
5. Lassen NA, Losen TS, Højgaard K, Skriver E. **Incomplete infarction: a CT-negative irreversible ischemic brain lesion.** *J Cereb Blood Flow Metab* 1983;3(suppl 1):S602–S603
6. Nakagawara J, Sperling B, Lassen NA. **Incomplete brain infarction of reperfused cortex may be quantitated with iomazenil.** *Stroke* 1997;28:124–132
7. Yamauchi H, Fukuyama H, Dong Y, et al. **Atrophy of the corpus callosum associated with a decrease in cortical benzodiazepine receptor in large cerebral arterial occlusive diseases.** *J Neurol Neurosurg Psychiatry* 2000;68:317–322
8. Kado H, Kimura H, Tsuchida T, et al. **Abnormal magnetization transfer ratios in normal-appearing white matter on conventional MR images of patients with occlusive cerebrovascular disease.** *Am J Neuroradiol* 2001;22:922–927
9. Basser PJ, Mattiello J, LeBihan D. **Estimation of the effective self-diffusion tensor from the NMR spin echo.** *J Magn Reson B* 1994;103:247–254
10. Buchsbaum MS, Tang CY, Peled S, et al. **MRI white matter diffusion anisotropy and PET metabolic rate in schizophrenia.** *Neuroreport* 1998;9:425–430
11. Werring DJ, Clark CA, Barker GJ, Thompson AJ, Miller DH. **Diffusion tensor imaging of lesions and normal-appearing white matter in multiple sclerosis.** *Neurology* 1999;52:1626–1632
12. Chabriat H, Pappata S, Poupon C, et al. **Clinical severity in CADASIL related to ultrastructural damage in white matter: in vivo study with diffusion tensor MRI.** *Stroke* 1999;30:2637–2643
13. Ellis CM, Simmons A, Jones DK, et al. **Diffusion tensor MRI assesses corticospinal tract damage in ALS.** *Neurology* 1999;53:1051–1058
14. Rose SE, Chen F, Chalk JB, et al. **Loss of connectivity in Alzheimer's disease: an evaluation of white matter tract integrity with colour-coded MR diffusion tensor imaging.** *J Neurol Neurosurg Psychiatry* 2000;69:528–530
15. Werring DJ, Toosy AT, Clark CA, et al. **Diffusion tensor imaging can detect and quantify corticospinal tract degeneration after stroke.** *J Neurol Neurosurg Psychiatry* 2000;69:269–272
16. Guo AC, Petrella JR, Kurtzberg J, Provenzale JM. **Evaluation of white matter anisotropy in Krabbe disease with diffusion tensor MR imaging: initial experience.** *Radiology* 2001;218:809–815
17. Pomara N, Crandall DT, Choi SJ, Johnson G, Lim KO. **White matter abnormalities in HIV-1 infection: a diffusion tensor imaging study.** *Psychiatry Res* 2001;106:15–24
18. O'Sullivan M, Summers PE, Jones DK, Jarosz JM, Williams SCR, Markus HS. **Normal-appearing white matter in ischemic leukoaraiosis: a diffusion tensor MRI study.** *Neurology* 2001;57:2307–2310
19. O'Sullivan M, Jones DK, Summers PE, Morris RG, Williams SCR, Markus HS. **Evidence for cortical "disconnection" as a mechanism of age-related cognitive decline.** *Neurology* 2001;57:632–638
20. Inglese M, Salvi F, Iannucci G, Manacardi GL, Mascalchi M, Filippi M. **Magnetization transfer and diffusion tensor MR imaging of acute disseminated encephalomyelitis.** *Am J Neuroradiol* 2002;23:267–272
21. Jones DK, Lythgoe D, Horsfield MA, Simmons A, Williams SCR, Markus HS. **Characterization of white matter damage in ischemic leukoaraiosis with diffusion tensor MRI.** *Stroke* 1999;30:393–397
22. Niendorf T, Dijkhuizen RM, Norris DG, van Lookeren Campagne M, Nicolay K. **Biexponential diffusion attenuation in various states of brain tissue: implications for diffusion-weighted imaging.** *Magn Reson Med* 1996;36:847–857
23. Assaf Y, Cohen Y. **Non-mono-exponential attenuation of water and N-acetyl aspartate signals due to diffusion in brain tissue.** *J Magn Reson* 1998;131:69–85
24. Mulkern RV, Gudbjartsson H, Westin CF, et al. **Multi-component apparent diffusion coefficients in human brain.** *NMR Biomed* 1999;12:51–62
25. Fazekas F, Chawluk JB, Alavi A, Hurtig HI, Zimmerman RA. **MR signal abnormalities at 1.5 T in Alzheimer's dementia and normal aging.** *Am J Roentgenol* 1987;149:351–356
26. Stejskal EO, Tanner JE. **Spin diffusion measurements: spin echoes in the presence of a time-dependent field gradient.** *J Chem Phys* 1965;42:288–292
27. Le Bihan D, Breton E, Lallemand D, Grenier P, Cabanis E, Laval-Jeantet M. **MR imaging of intravoxel incoherent motions: application to diffusion and perfusion in neurologic disorders.** *Radiology* 1986;161:401–407
28. Pierpaoli C, Basser PJ. **Toward a quantitative assessment of diffusion anisotropy [erratum appears in *Magn Reson Med* 1997;37:972].** *Magn Reson Med* 1996;36:893–906
29. Cao Y, Whalen S, Huang J, Berger KL, DeLano MC. **Asymmetry of subinsular anisotropy by in vivo diffusion tensor imaging.** *Hum Brain Mapp* 2003;20:82–90
30. Clark CA, Le Bihan D. **Water diffusion compartmentation and anisotropy at high b values in the human brain.** *Magn Reson Med* 2000;44:852–859
31. Yoshiura T, Mihara F, Tanaka A, et al. **High b value diffusion-weighted imaging is more sensitive to white matter degeneration in Alzheimer's disease.** *Neuroimage* 2003;20:413–419
32. Ueno M, Tomimoto H, Akiguchi I, Wakita H, Sakamoto H. **Blood-brain barrier disruption in white matter lesions in a rat model of chronic cerebral hypoperfusion.** *J Cereb Blood Flow Metab* 2002;22:97–104
33. Wakita H, Tomimoto H, Akiguchi I, et al. **Axonal damage and demyelination in the white matter after chronic cerebral hypoperfusion in the rat.** *Brain Res* 2002;924:63–70

HIGH LIGHT

Antiplatelet therapy contributes to acute deterioration of intracerebral hemorrhage

K. Toyoda, MD; Y. Okada, MD; K. Minematsu, MD; M. Kamouchi, MD; S. Fujimoto, MD; S. Ibayashi, MD; and T. Inoue, MD

Abstract—*Objective:* The purpose of this study was to examine the effect of antiplatelet therapy on the initial severity and the acute outcome of intracerebral hemorrhage (ICH). *Methods:* The authors reviewed records of 251 consecutive patients hospitalized in their cerebrovascular center within 24 hours after onset of ICH. *Results:* Fifty-seven patients (23%) had development of ICH during oral antiplatelet therapy. The major indication for antiplatelet therapy was the prevention of stroke recurrence (63%). As compared with patients without antiplatelet therapy, those who received antiplatelet therapy more frequently were aged 70 years or older (60% vs 35%; $p < 0.001$), had previous symptomatic ischemic stroke (54% vs 7%; $p < 0.0001$), had diabetes mellitus (26% vs 15%; $p < 0.05$), and had heart disease (32% vs 8%; $p < 0.0001$). Antiplatelet therapy was predictive of an increase in the hematoma volume by more than 40% on the second hospital day (hematoma enlargement, odds ratio [OR] 7.67, 95% CI 1.62 to 36.4) and the need for emergent surgical evacuation of the hematoma (OR 3.10, 95% CI 1.18 to 8.15). Antiplatelet therapy was an independent predictor for the occurrence of any of hematoma enlargement, emergent death, or evacuation surgery, which suggests that clinical deterioration occurs into the second hospital day (OR 7.45, 95% CI 2.46 to 22.5). *Conclusions:* Antiplatelet therapy seems to contribute to the acute clinical deterioration of intracerebral hemorrhage.

NEUROLOGY 2005;65:1000–1004

Oral anticoagulant therapy using warfarin increases the risk of intracerebral hemorrhage (ICH).[1] Patients with ICH during anticoagulant therapy have larger hematomas and worse outcomes than those not receiving anticoagulant therapy.[2,3] Similarly, meta-analyses have reported an increased risk of hemorrhagic stroke in patients using aspirin,[4,5] although another multicenter study did not confirm the increased risk of ICH with oral antiplatelet therapy.[6] The contribution of the antiplatelet therapy to the clinical severity of ICH has not yet been elucidated. Because oral antiplatelet agents are now used often in high-vascular-risk patients,[7] care should be exercised regarding their hemorrhagic complications. We sought to determine whether ICH occurring among patients taking oral antiplatelets had a worse clinical course in the acute stage vs patients not taking oral antiplatelets. We focused on the deterioration of ICH in the first 2 days, because this is the critical period when half of the 30-day mortality occurs and one-fourth of initially alert patients show a deterioration of consciousness.[8,9]

Additional material related to this article can be found on the *Neurology* Web site. Go to www.neurology.org and scroll down the Table of Contents for the October 11 issue to find the title link for this article.

Methods. We reviewed records of 303 consecutive patients with nontraumatic ICH who were hospitalized in our cerebrovascular center within 24 hours after stroke onset between January 1999 and February 2005. Of the 303 patients, 52 were ineligible for the study; 21 patients were taking warfarin; 7 were receiving IV heparin, urokinase, or ozagrel (an IV thromboxane A2-synthetase inhibitor) just before the onset of ICH; 1 had development of ICH during delivery; 1 was aged 9 years; 6 hemorrhaged primarily into the ventricles; 8 had an ICH due to aneurysmal rupture; and 8 had an ICH due to vascular malformations. The remaining 251 patients (152 men and 99 women aged 66 ± 12 years) served as subjects for the current study.

In all patients, ICH was verified by CT immediately after admission to our center (CT1). CT examinations were repeated approximately 24 hours later (day 2, CT2). The number, location, and volume of the hematomas as well as the ventricular bleeding and the time interval from ICH onset to CT1 were assessed. ICH volume was determined using the ABC/2 method by neuroradiologists blinded to the clinical history.[10] An increase in the volume by more than 40% between the two CTs was defined as hematoma enlargement.[11-14] This item was not assessed for patients who died

From the Departments of Cerebrovascular Disease (Drs. Toyoda, Okada, Kamouchi, and Fujimoto) and Neurosurgery (Dr. Inoue), Cerebrovascular Center and Clinical Research Institute, National Kyushu Medical Center, Fukuoka; Cerebrovascular Division, Department of Medicine, National Cardiovascular Center, Suita (Dr. Minematsu); and Department of Medicine and Clinical Science, Graduate School of Medical Sciences, Kyushu University, Fukuoka, Japan (Dr. Ibayashi).

Supported in part by the Research Grant for Cardiovascular Diseases (15C-1) from the Japanese Ministry of Health, Labor and Welfare.

Disclosure: The authors report no conflicts of interest.

Received November 11, 2004. Accepted in final form June 14, 2005.

Address correspondence and reprint requests to Dr. Kazunori Toyoda, Department of Cerebrovascular Disease and Clinical Research Institute, National Kyushu Medical Center, 1-8-1 Jigyohama, Chuo-ku, Fukuoka 810-8563, Japan; e-mail: toyoda@hsp.ncvc.go.jp

Table 1 *Comparison of clinical characteristics between patients with and without antiplatelet therapy*

	Antiplatelet (+), n = 57	Antiplatelet (−), n = 194	*p* Value
Baseline characteristics			
Age ≥70 y	34 (60%)	68 (35%)	<0.001
Previous symptomatic ICH	3 (5%)	26 (13%)	<0.1
Symptomatic ischemic stroke	31 (54%)	14 (7%)	<0.0001
Diabetes mellitus	15 (26%)	29 (15%)	<0.05
Heart disease	18 (32%)	16 (8%)	<0.0001
Physiologic status at admission			
Blood glucose >200 mg/dL	16 (28%)	33 (17%)	<0.07
CT findings			
Volume on CT1 >25 mL	25 (44%)	53 (27%)	<0.02
Volume on CT2 >25 mL*	6 (18%)	21 (14%)	NS
Acute outcome within 2 hospital days			
Emergent death	4 (7%)	10 (5%)	NS
Emergent evacuation surgery	20 (35%)	37 (19%)	<0.02
Hematoma enlargement >140%*	9 (27%)	12 (8%)	<0.005
Any of the above three items	33 (58%)	59 (30%)	<0.0005

* 24 patients in antiplatelet (+) and 47 patients in antiplatelet (−) were excluded.

ICH = intracerebral hemorrhage; NS = not significant.

or received surgical evacuation of the hematoma on the admission day (day 1).

Aspirin, ticlopidine, and cilostazol (a selective phosphodiesterase inhibitor) were included as target oral antiplatelets. Clopidogrel is not commercially used in Japan and was excluded from the analysis.

The following baseline characteristics were assessed: sex, age, previous symptomatic ICH, previous symptomatic ischemic stroke, hypertension (systolic blood pressure [SBP] ≥140/diastolic blood pressure [DBP] ≥90 mm Hg before ICH onset or history of antihypertensive medication), diabetes mellitus (fasting blood glucose ≥126 mg/dL, positive 75-g oral glucose tolerance test result, or history of antidiabetic medication), hypercholesterolemia (serum total cholesterol ≥220 mg/dL or history of antihypercholesterolemic medication), smoking habit, alcohol consumption, heart disease (including arrhythmia), liver disease, and neoplasm. As the physiologic status at admission, SBP, DBP, blood glucose, total cholesterol, platelets, fibrinogen, and activated partial thromboplastin time (APTT) were determined. Changes in SBP, DBP, and blood glucose during the first 2 days were also determined.

The neurologic deficits at admission were evaluated using the National Institutes of Health stroke scale (NIHSS) score. Activity of daily living before ICH was assessed by the modified Rankin scale (mRS) score.

Values are expressed as mean ± SD. Clinical characteristics of patients with ICH during oral antiplatelet treatment were compared with the remaining patients using a χ^2 test, unpaired Student's *t* test, and Mann–Whitney *U* test as appropriate. To assess initial ICH severity, we used the hematoma volume and the NIHSS score at admission. As indicators for acute deterioration of ICH, we assessed the emergent death and emergent surgical evacuation of the hematoma before the follow-up CT on day 2, and hematoma enlargement. To seek independent predictors for the above indicators, we performed multivariate logistic regression analysis using the clinical characteristics that showed a significant ($p < 0.05$) or a marginally significant ($0.05 \leq p < 0.1$) correlation with each indicator as independent variables by χ^2 test, with adjustments for sex and age. To investigate the time course of blood pressure and blood glucose, we performed one-way repeated-measures analysis of variance (ANOVA) and paired Student's *t* test for the comparison within a group, and two-way repeated-measures ANOVA for the comparison between groups.

Results. Among the 251 patients studied, 57 took oral antiplatelets daily before the onset of ICH; of these, 33 patients were taking 81 to 200 mg aspirin (81 mg in 16, 100 mg in 15, 162 mg in 1, and 200 mg in 1 patient); 12 were taking 100 to 300 mg ticlopidine (100 mg in 2, 200 mg in 9, and 300 mg in 1 patient); 3 were taking 100 mg cilostazol; 7 were taking both aspirin and ticlopidine (100 mg aspirin and 100 mg ticlopidine in 2, and 81 mg aspirin and 200 mg ticlopidine in 5 patients); 1 was taking both aspirin (100 mg) and cilostazol (100 mg); and 1 was taking both ticlopidine (200 mg) and cilostazol (200 mg). The indications for antiplatelet therapy included cardioembolic ischemic stroke in 4, noncardioembolic ischemic stroke in 32, nonvalvular atrial fibrillation without previous stroke in 4, ischemic heart disease without previous stroke in 8, and other peripheral vascular diseases in 9.

Of the baseline characteristics, age 70 years or older ($p < 0.001$), previous symptomatic ischemic stroke ($p < 0.0001$), diabetes mellitus ($p < 0.05$), and heart disease ($p < 0.0001$) were more frequent in patients taking antiplatelets than in those not taking antiplatelets (table 1; more detailed data are provided in table E-1 on the *Neurology* Web site at www.neurology.org). At admission, blood glucose greater than 200 mg/dL tended to be more frequent ($p < 0.07$), and the value of blood glucose was higher ($p < 0.02$) in patients with than without antiplatelets. In both patients with and patients without antiplatelets, SBP ($p < 0.0001$), DBP ($p < 0.0001$), and blood glucose ($p < 0.001$) became lower to the reference range during the first 2 days (figure).

The volume of the hematoma on CT1 varied from 0.3 to 252 mL (median 10.5 mL) and more frequently exceeded 25 mL in patients with than patients without antiplatelets ($p < 0.02$). The volume on CT2, varying from 0.4 to 210 mL